nature research

https://doi.org/10.1038/s41550-020-1183-3

Supplementary information

Optical follow-up of the neutron star–black hole mergers S200105ae and S200115j

In the format provided by the authors and unedited

Supplemental Information for "Optical follow-up of the neutron star-black hole mergers S200105ae and S200115j"

Shreya Anand[1,*], Michael W. Coughlin[1,2*], Mansi M. Kasliwal[1], Mattia Bulla[3], Tomás Ahumada[4], Ana Sagués Carracedo[5], Mouza Almualla[6], Igor Andreoni[1], Robert Stein[7,8], Francois Foucart[9], Leo P. Singer[10,11], Jesper Sollerman[12], Eric C. Bellm[13], Bryce Bolin[1], M. D. Caballero-García[14], Alberto J. Castro-Tirado[15,16], S. Bradley Cenko[10,11], Kishalay De[1], Richard G. Dekany[17], Dmitry A. Duev[1], Michael Feeney[17], Christoffer Fremling[1], Daniel A. Goldstein[1], V. Zach Golkhou[13,18], Matthew J. Graham[1], Nidhal Guessoum[6], Matthew J. Hankins[1], Youdong Hu[15,19], Albert K. H. Kong[20], Erik C. Kool[12], S. R. Kulkarni[1], Harsh Kumar[21], Russ R. Laher[22], Frank J. Masci[22], Przemek Mróz[1], Samaya Nissanke[23] Michael Porter[17], Simeon Reusch[7,8], Reed Riddle[17], Philippe Rosnet[24], Ben Rusholme[22], Eugene Serabyn[25], R. Sánchez-Ramírez[26], Mickael Rigault[24], David L. Shupe[22], Roger Smith[17], Maayane T. Soumagnac[27,28], Richard Walters[17] and Azamat F. Valeev[29]

[1]*Division of Physics, Mathematics, and Astronomy, California Institute of Technology, Pasadena, CA 91125, USA*

[2]*School of Physics and Astronomy, University of Minnesota, Minneapolis, Minnesota 55455, USA*

[3]*Nordita, KTH Royal Institute of Technology and Stockholm University, Roslagstullsbacken 23, SE-106 91 Stockholm, Sweden*

[4]*Department of Astronomy, University of Maryland, College Park, MD 20742, USA*

[5]*The Oskar Klein Centre, Department of Physics, Stockholm University, AlbaNova, SE-106 91 Stockholm, Sweden*

[6]*American University of Sharjah, Physics Department, PO Box 26666, Sharjah, UAE*

[7]*Deutsches Elektronen Synchrotron DESY, Platanenallee 6, 15738 Zeuthen, Germany*

[8]*Institut für Physik, Humboldt-Universität zu Berlin, D-12489 Berlin, Germany*

[9]*Department of Physics, University of New Hampshire, 9 Library Way, Durham NH 03824, USA*

[10]*Astrophysics Science Division, NASA Goddard Space Flight Center, MC 661, Greenbelt, MD 20771, USA*

[11]*Joint Space-Science Institute, University of Maryland, College Park, MD 20742, USA*

[12]*The Oskar Klein Centre, Department of Astronomy, Stockholm University, AlbaNova, SE-106 91 Stockholm, Sweden*

[*] These two authors contributed equally to this work.

[13]DIRAC Institute, Department of Astronomy, University of Washington, 3910 15th Avenue NE, Seattle, WA 98195, USA
[14]Astronomical Institute of the Academy of Sciences, Bocní II 1401, CZ-14100 Praha 4, Czech Republic.
[15]Instituto de Astrofísica de Andalucía (IAA-CSIC), Glorieta de la Astronomía s/n, E-18008, Granada, Spain
[16]Departamento de Ingeniería de Sistemas y Automática, Escuela de Ingenieros Industriales, Universidad de Málaga, Unidad Asociada al CSIC, C. Dr. Ortiz Ramos sn, 29071 Málaga, Spain
[17]Caltech Optical Observatories, California Institute of Technology, Pasadena, CA 91125, USA
[18]The eScience Institute, University of Washington, Seattle, WA 98195, USA
[19]Universidad de Granada, Facultad de Ciencias Campus Fuentenueva S/N CP 18071 Granada, Spain
[20]Institute of Astronomy, National Tsing Hua University, Hsinchu 30013, Taiwan
[21]Indian Institute of Technology Bombay, Powai, Mumbai 400076, India
[22]IPAC, California Institute of Technology, 1200 E. California Blvd, Pasadena, CA 91125, USA
[23]Center of Excellence in Gravitation and Astroparticle Physics, University of Amsterdam, Netherlands
[24]Université Clermont Auvergne, CNRS/IN2P3, Laboratoire de Physique de Clermont, F-63000 Clermont-Ferrand, France
[25]Jet Propulsion Laboratory, California Institute of Technology, Pasadena, CA 91109, USA
[26]INAF - Instituto di Astrofisica e Planetologia Spaziali, Via Fosso del Cavaliere 100, 00133 Roma, Italy.
[27]Lawrence Berkeley National Laboratory, 1 Cyclotron Road, Berkeley, CA 94720, USA
[28]Department of Particle Physics and Astrophysics, Weizmann Institute of Science, Rehovot 76100, Israel
[29]Special Astrophysical Observatory, Russian Academy of Sciences, Nizhnii Arkhyz, 369167 Russia

1 Observational details

Photometric Observations The ZTF observations used to discover potential candidates were primarily obtained with ToO program time, however the public survey [1] provided us with data as

well. The nominal exposure time for the ZTF public survey is 30s while for the ToO program varies from 120-300 s depending on the available time and sky area requiring coverage. Our first source of photometry comes from the ZTF alert production pipeline [2], however for the purposes of this paper we have performed forced photometry using the package `ForcePhot`[3] on the candidates and reported these values.

For S200105ae, we split the schedule into two blocks of right ascension due to the significantly displaced lobes in the skymap, with observations lasting three hours per block. We additionally utilized the "filter balancing" feature [4], which optimizes for the number of fields that have observations scheduled in all requested filters, and employed the greedy-slew algorithm [5] for conducting our search. The ability to split the skymap in right ascension and the use of filter balancing was novel for these observations, and served to help address the previous difficulty with multi-lobed skymaps to make it possible to observe all filters requested for the scheduled fields. Previously, maps of this type created conflicts between the rising/setting times of the lobes, as well as the separation in time between each of the epochs. This problem impacts the transient filtering process as well, for example, resulting in a number of transients failing to satisfy the criteria of 15 minutes between consecutive detections to reject asteroids. With the implementation of these features, both g- and r-band epochs were successfully scheduled for almost all fields.

For photometric follow-up we used the Gemini Multi-Object Spectrograph (GMOS-N)[6] on the Gemini-North 8-meter telescope on Mauna Kea, the Spectral Energy Distribution Machine (SEDM) on the Palomar 60-inch telescope [7], the Wide-field Infrared Camera (WIRC)[8] on the Palomar 200-inch telescope, as well as telescopes that are part of the Las Cumbres Observatory (LCO) network and the Kitt Peak EMCCD Demonstrator (KPED)[9].

The LCO observations were scheduled using the LCO Observation Portal (`https://observe.lco.global/`), an online platform designed to coordinate observations. Our imaging plans changed case by case, however our standard requests involved 3 sets of 300s in g- and r- band with the 1-m telescopes. For fainter sources we requested 300s of g- and r- band with the 2-m telescopes. The reduced images available from the Observation Portal were later stacked and sources were extracted with the SourceExtractor package[10]. We calibrated magnitudes against Pan-STARRS1[11] sources in the field. For transients separated $< 8''$ from their hosts, we aligned a cutout of the transient with a Pan-STARRS1 template using SCAMP[12] and performed image

subtraction with the High Order Transform of Psf ANd Template Subtraction (HOTPANTS) code [13], an enhanced version of the method derived by Ref. [14]. Photometry for these candidates comes from an analogous analysis on the residual images. Furthermore, images obtained with the Liverpool telescope (LT)[15] were reduced, calibrated and analysed in a similar fashion.

For KPED data, our standard procedure is to stack an hour of r-band data and reduce the stacked images following to standard bias and flat field calibrations. The photometry is obtained following the same methods as for the LCO data.

The photometric data obtained with GMOS-N was split in four 200 s g-band images later combined and reduced with DRAGONS (`https://dragons.readthedocs.io/en/stable/`), a Python-base data reduction platform provided by the Gemini Observatory. The data were later calibrated using the methods described for LCO.

Additionally, we scheduled photometric observations with the SEDM automatically through the GROWTH marshal. We acquired g-, r-, and i- band imaging with the Rainbow Camera on SEDM in 300s exposures. SEDM employs a python-based pipeline that performs standard photometric reduction techniques and uses an adaptation of `FPipe` (Fremling Automated Pipeline; described in detail in Ref. [16]) for difference imaging. Data are automatically uploaded to the GROWTH marshal after having been reduced and calibrated.

The near-infrared data obtained with WIRC were reduced using a custom data reduction pipeline described in Ref. [17], and involved dark subtraction followed by flat-fielding using sky-flats. The images were then stacked using Swarp [18] and photometric calibration was performed against the 2MASS point source catalog [19]. Reported magnitudes were derived by performing aperture photometry at the location of the transient using an aperture matched to the seeing at the time of observation, including an aperture correction to infinite radius.

The photometry presented in the light-curves on this paper was corrected for galactic extinction using dust maps from Ref. [20].

Spectroscopic Observations For the candidate dataset described in Sec. 2, we obtained spectroscopic data using the Gran Telescopio Canarias (GTC) and Palomar observatory. We obtained optical

spectra of one set of candidates with the 10.4-meter GTC telescope (equipped with OSIRIS). Observations made use of the R1000B and R500R grisms, using typically a slit of width 1.2″. Data reduction was performed using standard routines from the Image Reduction and Analysis Facility (IRAF).

For the second set of candidates, we acquired most of our spectra with the Integral Field Unit (IFU) on SEDM, a robotic spectrograph on the Palomar 60-inch telescope [7]. We scheduled spectroscopic observations for our brighter ($m_{AB} < 19$) and higher priority targets using a tool on the GROWTH Marshal that directly adds the target to the SEDM queue. For each science target, the SEDM robot obtains an acquisition image, solves the astrometry and then sets the target at the center of the integral field unit field of view. At the end of exposure, the automated pysedm pipeline is run [21]. It first extracts the IFU spaxel tracers into a x,y,λ cube accounting for instrument flexures; the target spectrum is then extracted from the cube using a 3D PSF model which accounts for atmospheric differential refractions. The spectrum is finally flux calibrated using the most recent standard star observation of the night, with the telluric absorption lines scaled for the target's airmass. See Ref. [21] for more details on the reduction pipeline. The final extracted spectra are then uploaded to the marshal; we use the SNID software [22] to classify our transients.

Using the Double Spectrograph (DBSP) on the Palomar 200-inch telescope we obtained one transient and one host galaxy spectrum during our classical observing run on 2020-01-18 UT. For the setup configuration, we use 1.0″and 1.5″slitmasks, a D55 dichroic, a B grating of 600/4000 and R grating of 316/7500. Data were reduced using a custom PyRAF DBSP reduction pipeline (https://github.com/ebellm/pyraf-dbsp) [23].

2 Candidates

S200105ae candidates In this subsection, we provide brief descriptions of candidates identified within the skymap of S200105ae. Due to the poor seeing conditions and moon brightness, there were no candidates that passed all of the criteria after the second night of observations. After the third night of observations of S200105ae, we identified 5 candidates within the skymap [24], shown in Supplementary Information Table 1. In addition, we later identified and reported other candidate counterparts [25]. A late-time query (> 1 month after the mergers) yielded two further candidates of interest, ZTF20aafsnux and ZTF20aaegqfp, that were not already reported via Gamma-ray burst

Coordinates Network (GCN).

All the transients are displayed in Supplementary Information Table 2; here we briefly describe each set, and show examples of light curves and cutouts for the most well-sampled, slowly photometrically evolving ones in Supplementary Information Figure 1. For the candidates with spectroscopic redshifts, we compute their distance assuming Planck15 cosmological parameters and use them to estimate the source absolute magnitudes, which we include in the candidate descriptions. When vetting, we prioritized candidates whose distance fell within the 1σ LIGO distance uncertainty for each event; however we did not reject any candidates on the basis of redshift.

The redshifts presented in this section come either from the spectra of the transient, z(s), or from the Photometric Redshifts for the Legacy Surveys (PRLS) catalog (Zhou et al. in prep.), which is based on Data Release 8 of DESI Legacy Imaging Surveys [26], z(p).

Spectroscopic Classification

For this set of spectra, we quote the photometric phase at which the spectrum was taken when the photometry is well-sampled. In all other cases, we derive the spectroscopic phase of the transient using SNID [22] unless otherwise specified. Most of the spectroscopic classifications were determined using SNID.

ZTF20aaertpj - The first r- and g-band detections of this transient 3 days after the merger showed a red color $g-r$ = 0.4 mag; it rapidly brightened 1 mag to reach g = 18.9 after 7 days. The Gran Telescopio Canarias (GTC) classified it as a Type Ib SN (z(s) = 0.026) on January 10th [27] a few days before the ZTF lightcurve reached maximum light, implying an absolute magnitude of -15.9 mag. This supernova is closer than the -1σ LIGO distance.

ZTF20aaervoa - This object was found 3 days after the merger at 20.74 mag in g band with a red color ($g-r=0.66$ mag). This field was last observed 1.6 days before the merger. It showed a flat evolution over the first few days. Spectroscopic follow-up with GTC on January 10th classified it as a SN Type IIP (z(s) = 0.046), $\sim$ 3 days after maximum [28] using SNID templates. This implied

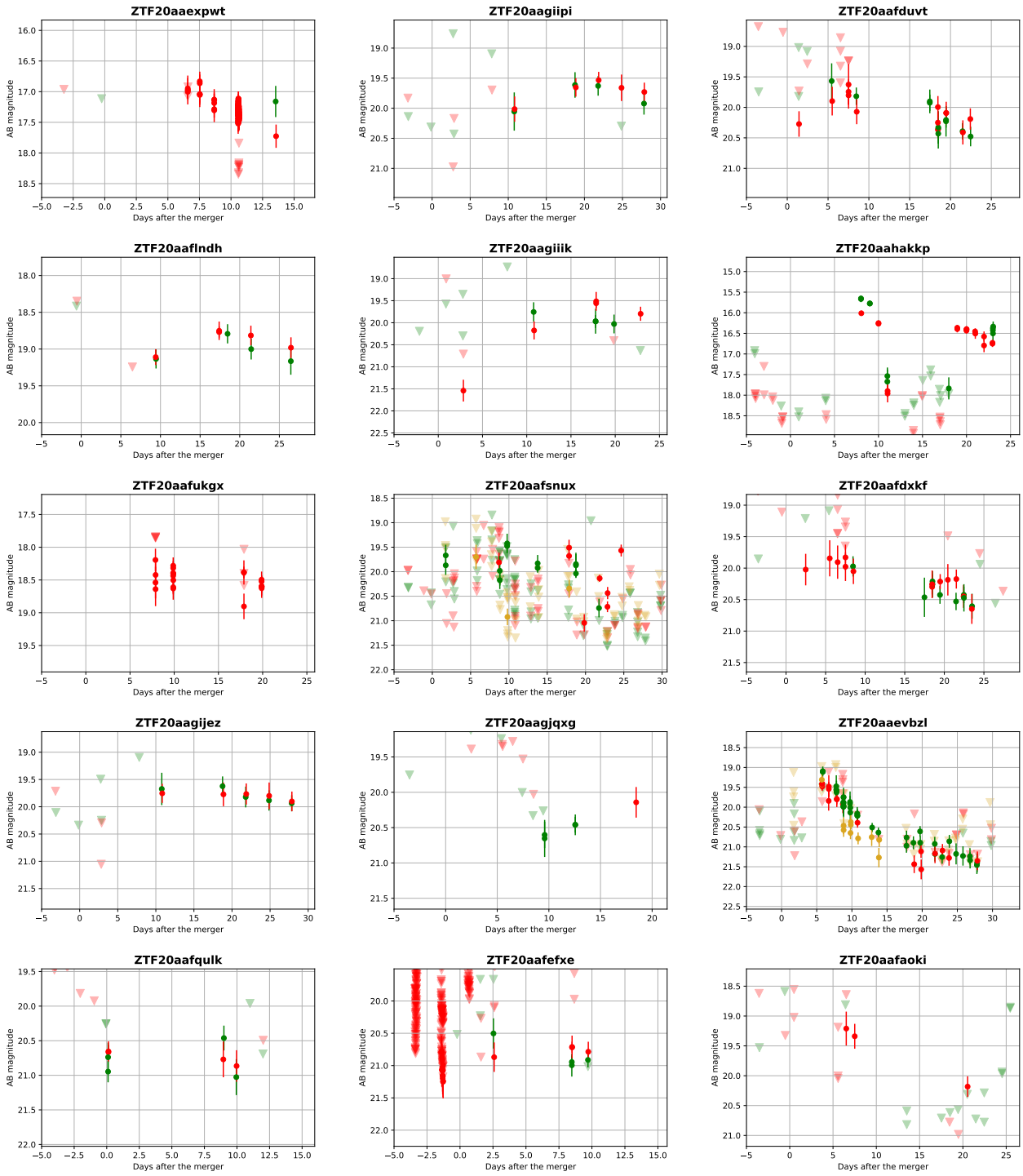

Supplementary Information Figure 1: **Lightcurves for all objects ruled out photometrically.** In each panel, filled circles represent ZTF forced photometry and the photometry from the ZTF alert production pipeline, with error bars corresponding to 1-σ uncertainties. Filled triangles display 5-σ upper limits for non-detections. The r-, g-, and i-band data is presented in red, green and yellow respectively.

an absolute magnitude of -16.4 mag in r band. Its redshift is marginally consistent with the LIGO distance uncertainty, though it fell outside the 95% confidence level of the LALInference skymap.

ZTF20aaervyn - Its first detection was in the g band (g = 20.62 mag), 3 days after the merger, which first showed a red color ($g - r = 0.3$ mag). This field was last visited 3 hours before the LVC alert. It was classified by GTC on Janunary 11th as a Type Ia SN, with z(s) = 0.1146 [28], much farther than $+1\sigma$ LIGO distance. The spectroscopic phase corresponds to $\gtrsim 1$ week before the lightcurve reached maximum light.

ZTF20aaerxsd - Similarly, this region was visited 3 hours before the LVC alert and this candidate was first detected 3 days after the merger at g = 20.27 mag and showed a red color of $g - r$ = 0.37 mag. The next couple of detections showed a quickly evolving transient, brightening ~ 0.35 mag/day. GTC spectroscopically classified it as a SN Type Ia (z(s) = 0.0533) on January 10th [28]; concurrent photometry with ZTF indicates that the spectrum was taken > 12 days before maximum.

ZTF20aaerqbx - This transient was first detected in g-band at g = 19.46 mag 3 days after the merger. It faded 0.5 mag over the first 8 days and was classified by GTC on January 11th as a Type IIP SN (z(s) = 0.098) at 5 days before maximum, using SNID [27]. Its redshift places it outside of the LIGO volume.

ZTF20aafanxk - This candidate was detected at r = 18.52 mag, 6 days after the merger with galactic latitude $< 15^\circ$ and offset by $7''$ from a possible host [25]; it faded 0.3 mag in the r-band the first 10 days and a spectrum taken with the P60 SEDM spectrograph revealed its classification to be a SN Ia at z(s) = 0.103, too far to be consistent with the LIGO distance.

ZTF20aafujqk - Offset by $2.26''$ from the center of a large spiral galaxy host [25], ZTF20aafujqk was detected in r-band during serendipitous observations 10 days after the merger, and later followed up with SEDM photometry in g- and i- bands, which showed a steadily declining lightcurve. SEDM spectroscopy showed that it was also a SN Ia at z(s) = 0.06, consistent with LIGO distance uncertainties.

ZTF20aaevbzl - This region was last observed 3 hours before the LVC alert. ZTF20aaevbzl

was detected six days after the merger [25], this candidate was selected for its atypical rapid decline in its lightcurve in r- and g-bands. This hostless transient faded 1.1 mag in 5 days in the g-band. We obtained a spectrum of ZTF20aaevbzl with P200+DBSP, whose Hα feature at z(s) = 0 amidst a blue, mostly featureless spectrum indicates that it is a galactic cataclysmic variable (See Figure 2 in Main Text). Further follow-up with SEDM and LCO showed that the transient was consistently fading at 0.18 magnitudes per day in the g- band.

(Slow) Photometric Evolution

As mentioned above, we deem candidates to be slowly evolving by checking whether their rise or decay rate is faster than our photometric cut of $< |0.3|$ mag/day. We justify this cut based on Supplementary Information Figure 2, a histogram of the evolution rates of KNe from NSBH mergers, which shows that over a baseline of $\gtrsim$1 week, which is the case for our candidates, nearly all KN model lightcurves evolve faster than this cut in both g- and r-bands. The decline rate is determined using the photometric band with the longest available baseline. It is calculated by getting the ratio between the Δm and the length of that baseline (Δt), from the candidate's peak to its last detection. This cut does exclude from our analysis a small part of the physically acceptable parameter space of NSBH binaries, though it significantly reduced the number of false-positive transients. It should thus be seen as a trade-off between parameter space coverage and the cost of EM follow-up that result in a small and known bias in our search.

ZTF20aafduvt - The field where this transient lies was observed 12 hours before the LVC alert, and it was detected six days after the merger in r- and g- bands [25], offset from a possible host at z(p) = 0.21 ± 0.02 by 51kpc, this candidate faded 0.1 mag in the g-band during the first 9 days after the discovery. The photometric redshift places this transient at an absolute magnitude of M = -21.

ZTF20aaflndh - With its last non-detection 12 hours before the GW alert, ZTF20aaflndh was first detected 10 days after the merger. This source is located $0.8''$ from the center of an apparently small galaxy [25] and evolved photometrically to resemble a Type Ia SN light curve; it faded in the r-band by 0.17 mag in 17 days. Furthermore, the photo-z of the host galaxy is z(p) = 0.091 $\pm$ 0.023 which puts the transient at an absolute magnitude of M = -19.06 mag, consistent with a Type

Ia SN.

ZTF20aaexpwt - This candidate was first detected one week post-merger, and was one of several hostless candidates identified in a low galactic latitude ($b_{gal} < 15°$) field [25]. The last non-detection was 5 hours before the LVC alert. Its evolution over the next seven days was 0.12 mag/day in the r-band, marked by a declining lightcurve.

ZTF20aafukgx - Offset from a potential bright host by 3.85″, at low galactic latitude [25], this candidate was detected at r = 18.4 ten days after the merger but remained flat within error-bars over the next ten days of observations.

ZTF20aagijez - First detected 11 days post-merger, this candidate, offset 3.15″ from the nucleus of a star-forming galaxy at z(s) = 0.061 [25], exhibited a flat lightcurve for more than 10 days and it was still detectable after 40 days; it photometrically resembles a SN light curve. The spectroscopic host redshift implies an absolute magnitude of M = -17.6 mag. The last visit to the field where this transient lies was 3.6 hours before the GW alert.

ZTF20aagiiik - This field was last visited 2 days before the LVC alert. We identified ZTF20aagiiik as a candidate of interest due to its rapid rise in r-band after being detected 11 days after the merger; it is offset by 5.79″ from a potential spiral galaxy host [25]. However, it only faded 0.4 mag in 12 days. Additionally, at the redshift of the potential host galaxy (z(s) = 0.13, separated by 5.25″) the absolute magnitude (M = -19.24 mag) is consistent with a Type Ia SN.

ZTF20aafdxkf - Detected just three days after the merger, this hostless candidate exhibited a rise in r-band over the first three days [25], but its declining g-band photometry showed it to be too slow to be a KN. It only faded 0.5 mag in the g-band during the first 14 days. The last non-detection was 12 hours before the LVC alert.

ZTF20aagiipi - Offset by 27 kpc from a potential faint host at z(p) = 0.388 ± 0.016, this candidate seemed to be rising when it was detected in the first 11 days after merger. Supplemented with SEDM photometry, its lightcurve closely resembles that of a typical Type Ia supernova, which at the redshift of the host would peak at M = -21.6 mag. This field was last observed 3.6 hrs before the LVC alert.

ZTF20aafsnux - A hostless candidate, ZTF20aafsnux appeared to be declining gradually based on its first two g-band detections two and nine days after the merger. Close monitoring revealed that the source was fluctuating between $g \sim 19.0$–20.0 mag over a period of 17 days. This region was last visited 3 hours before the GW alert.

ZTF20aaertil - This candidate was first detected three days after the merger; it was located $0.2''$from the nucleus of a faint galaxy host and appeared to be rising in g-band [25]. Our spectrum of the host galaxy with DBSP on Jan 18th demonstrated that the galaxy, at z(s) = 0.093, was outside the one-sigma distance uncertainty for S200105ae; furthermore, in 40 days, it faded only 0.5 mag in the r-band. The absolute magnitude at this host redshift is M = -18.5 mag. We show the lightcurve and r-band cutouts for this transient in Supplementary Information Figure 4. The last non-detection in this field was 3 hours before the LVC alert.

ZTF20aafksha - This last non-detection for this transient was 1.2 days before the GW alert. We discovered this candidate nine days after the merger, offset by $7.92''$ from a possible spiral galaxy host at z(s) = 0.167 at g = 20.06 mag [25], corresponding to an absolute magnitude of about -19.6 mag. The steadily declining lightcurve post-peak in both g-band and r-band, 0.7 mag in g-band during the first 19 days, and the bright absolute magnitude, suggests that the candidate is a SN Ia. We display this candidate in Supplementary Information Figure 4.

ZTF20aagjemb - First detected 3 days after merger, this nuclear candidate rose by one magnitude over the course of 5 days in g-band [25]. After tracking its evolution over 20 days time, the lightcurve seems to exhibits a SN-like rise and decline. It presents a slowly-evolving lightcurve, only fading 0.1 mag in the r-band during the twenty days. This candidate is also displayed in Supplementary Information Figure 4. The transient is located in a host with a z(p) = 0.21 $\pm$ 0.06, separated by 6 kpc, implying an absolute magnitude M = -19.24 mag. The last non-detection in this region was 3 hours before the LVC alert.

ZTF20aafefxe - This candidate's two detections in r-band suggest fading behaviour, but subsequently the source has not been detected by the nominal survey observations [25]. The last non-detection in this region was 5 hours before the LVC alert. The first detection was 9 days after the merger, and there may be a faint host separated by 41 kpc from the transient with z(p) = 0.09 $\pm$ 0.05, indicating a luminosity of $M = -17.2$ mag. Forced photometry revealed that it had only

evolved 0.16 mags in 11 days in the g-band, placing it clearly into the category of slow evolvers.

ZTF20aafaoki - The last non-detection in this region was 12 hours before the LVC alert. This candidate had two r-band detections at 19.2 mag, but had faded below 21.4 mag just 5 days later [25]. Our images taken with KPED do not show any transient or background source up to $g > 19.55$ mag 6 days after the discovery. Similarly, our LCO follow-up observations showed that 8 days after the discovery, the transient is not detected and there is no visible source at the corresponding coordinate up to $g > 20.25$ mag and $r > 21.6$ mag. Our last LCO observations, obtained 72 days after the discovery, show no transient up to $g > 22.10$ mag. However, after running forced photometry at the transient position, we find a detection 14 days after the initial discovery at r = 21.2 mag, implying re-brightening of the transient after the non-detection upper limits, or very slow evolution.

Stellar

ZTF20aafexle - This particular region was observed serendipitously 1 hour before the LVC alert. After its initial detection 8 days after the merger, it brightened by nearly one magnitude over four days but returned to its original brightness after 5 days [25]. We posit that it may be stellar due to the PS1 detections at the source position. Additionally, its evolution over the first 10 days after the discovery is only 0.3 mag in the r-band.

Slow-moving asteroids

ZTF20aaegqfp - We detected this hostless candidate a day after the merger in r band. The last non-detection of this transient was 5 hours before the GW alert. Our pipelines identified it as a fast-evolving transient due to its rise by more than 0.5 mag over the course of the night; subsequently, it was not detected in any our serendipitous observations. We find non-physical upper limits interspersed with detections, suggesting that the photometry for this transient may not be reliable. Using the Kowalski infrastructure, we queried for alerts in the vicinity of the transient (around 25″) and found 13 alerts, the oldest of which was ~ 4 days before the trigger, which showed a moving

object across the field alerts (see Supplementary Information Figure 3).

S200115j candidates In this subsection, we provide brief descriptions of candidates identified within the skymap of S200115j. Most of our candidates were identified during the serendipitous coverage of the map. Some of our transients were discovered within ZTF Uniform Depth Survey (ZUDS; Goldstein et al., in prep) a dedicated survey for catching high-redshift SNe by acquiring and stacking images to achieve greater depth compared to the nominal survey. Intrinsically faint transients ($m_{\rm AB} \sim -16$ mag) discovered in these fields are more likely to be at redshifts consistent with the distance of this event (340 ± 79 Mpc).

The relevant candidates circulated by the GROWTH collaboration [29] were found on the first night of observations. Weather issues affected systematic follow-up in the following days; nevertheless, a later deeper search led to more candidates found to be temporally and spatially consistent, which we report here. Additionally, candidates from Ref. [30] were cross-matched with the ZTF database in order to temporally constrain the transients. Only S200115j_X136 [30] had an optical counterpart we could identify, ZTF20aafapey, with a flaring AGN [31].

Every candidate that was found in the region of interest is listed in Supplementary Information Table 3.

Spectroscopic Classification

ZTF20aafqpum - This transient is located at the edge of a host galaxy at photz $= 0.12 \pm 0.03$ [29]. The region was last observed 1 hour before the LVC trigger and the transient. Follow-up with the Liverpool telescope in r- and i-bands showed this candidate to be red, with $g - r \sim 0.5$ mag. This transient was then spectroscopically classified by ePESSTO+ as a SN Ia 91-bg, at z(s) = 0.09 [32], placing it at an absolute magnitude of $M = -17.3$ mag.

(Slow) Photometric Evolution

ZTF20aahenrt - This candidate, detected during our serendipitous search 3 days after the merger, is separated from a galaxy host by 8.8 kpc at z(p) = 0.16 $\pm$ 0.04, giving it an absolute magnitude of $M = -15.6$ mag. We monitored the transient after its initial rise in g-band, but over 12 days the candidate lightcurve exhibits very flat evolution, rising by 0.14 mag in 7 days. We highlight it in Supplementary Information Figure 4 as an example of a very slowly evolving transient identified in our searches. This field was serendipitously observed 30 min before the LVC alert.

ZTF20aagjqxg - We selected this hostless candidate during our scanning due to its faint g-band detection at g = 20.65 mag and subsequent rise three days after the initial detection two hours after the merger; its detection 11 days later in the r-band suggests that it was rising or reddening at a rate of < 0.1 mag/day. This field was last observed 3.5 days before the LVC alert.

ZTF20aahakkp - This hostless transient was first detected eight days after the merger in g = 15.67 mag and r = 16.01 mag. The last non- detection of this transient was 20 hours before the issue of the LVC alert. While the transient seems to be rapidly fading over the course of a day from r = 16.26 mag to r = 17.9 mag, this detection is likely affected by poor weather and bad seeing on that day (seeing 4″). 20 days later, the lightcurve is near the original detection magnitude, and exhibits a slow fade since then.

ZTF20aafqulk - This region was last observed 1 hour before the issue of the GW alert. This source was detected 2.5 hours after the merger in g-band and 43 minutes later in r-band, with a blue color (g-r = 0.2 mag).The candidate is offset by 0.3″ from a potential host galaxy at a photometric redshift of z(p) = 0.27 $\pm$ 0.04 [29]. Our P60+SEDM spectrum does not offer a clear classification, but we detect a source in our LCO images 5 days after its discovery with $r = 20.16 \pm 0.1$ mag. When running forced photometry, we find a detection in the r-band 89 days before the trigger, definitively ruling out its association with the GW event. Furthermore, the lightcurve appears nearly flat in the r-band over the course of 10 days.

Slow-moving asteroids

Solar System asteroids located in the proximity of the stationary points located at $\sim 60^\circ$ from opposition and low ecliptic latitude [33] have slow, $\lesssim 1''$/h sky motions [34].

ZTF20aafqvyc - This was first detected as a hostless candidate 2.5 hours after the merger in g-band, followed by a detection in r-band just 49 minutes later [29]. Due to the transient being faint at g = 20.39 mag, with a $g-r$ color of 0.34 mag, we pursued follow-up with P200+WIRC on 2020-01-18 with NIR non-detections down to $J > 21.5$ mag and $K_s > 20.9$ mag [35] and LCO on 2020-01-19 with optical non-detections down to $g > 22.6$ mag, $r > 21.8$ mag and $i > 20.9$ mag [36]. Follow-up reported with AZT-33IK telescope of Sayan observatory (Mondy) revealed non-detections just 13 hours and one day after the merger, down to upper limits of 21.6 mag and 22.1 mag in the r-band, suggesting that the source could be fast-fading, if astrophysical [37]. Finally, we conducted follow-up with Gemini GMOS-N, detecting no source down to an upper limit of $g > 24.5$ mag [38]. Based on the puzzling non-detections, we investigated the possibilities that it could be an artifact or that it was a moving object. Close inspection of the images taken with the Liverpool Telescope, 12.9 hours after the merger in g- and r-bands clearly demonstrated that the object had shifted position in the image with a slow angular rate of motion consistent with being an asteroid with an opposition-centric location of $\pm 60^\circ$ near the evening sky stationary point.

3 Ejecta mass and binary parameter constraints – Implications and caveats

To further illustrate what we could learn from sufficiently deep observations, we consider potential constraints on the parameters of the NSBH binary powering S200105ae. We assume that the source was located at $283\,\mathrm{Mpc}$, and seen face-on. For the deepest fields reported here, we have seen that this implies $M_{\rm ej,dyn} \lesssim 0.02\,M_\odot$ and $M_{\rm ej,pm} \lesssim 0.04\,M_\odot$. Using semi-analytical formulae calibrated to the results of numerical simulations, we can estimate $M_{\rm ej,dyn}$ and $M_{\rm ej,pm}$ as functions of the mass ratio of the binary ($Q = M_{\rm BH}/M_{\rm NS}$), the component of the dimensionless black hole spin aligned with the orbital angular momentum (χ), and the neutron star compactness ($C_{\rm NS} = \frac{GM_{\rm NS}}{R_{\rm NS}c^2}$) (see also Refs. [39–44]). We compute $M_{\rm ej,pm}$ using Ref. [45], and $M_{\rm rem}$ using Ref. [46], which are based on, respectively, the work of Ref. [47] and Ref. [48]. As Ref. [45] only predicts the total mass remaining outside of the BH after merger, $M_{\rm rem}$, we estimate $M_{\rm ej,pm} = f_{\rm rem}(M_{\rm rem} - M_{\rm ej,dyn})$,with

$f_{\rm rem} \sim 0.15 - 0.5$ the fraction of the remnant accretion disk that is ejected in the form of disk winds [49]. The results are shown in Extended Data Figure 7, expressed as the maximum BH spin compatible with the assumed mass constraints. We show results for $f_{\rm rem} = 0.15$ and $f_{\rm rem} = 0.5$, to illustrate the dependence on the (poorly constrained) parameters. While our plots show results at a fixed $M_{\rm NS} = 1.35\,M_\odot$, they can easily be rescaled to any other choice for the neutron star mass, as the mass predictions only depend on the ratio $M_{\rm NS}/R_{\rm NS}$. We note that at high mass ratios, the choice of $f_{\rm rem}$ has nearly no impact on the constraints. This occurs because the limit on $M_{\rm ej,dyn}$ is more constraining than the limit on $M_{\rm ej,pm}$. At lower mass ratios, on the other hand, $M_{\rm ej,dyn}$ rapidly decreases (it asymptotes to the low values predicted for BNS systems in the near equal-mass regime). In that regime, the choice of $f_{\rm rem}$ clearly impacts the constraints that we can place on the binary parameters. Conservative upper limits on the BH spin are obtained by choosing $f_{\rm rem} \sim 0.15$. Should more detailed study of post-merger remnants reveal that higher values of $f_{\rm rem}$ are more realistic, our constraints could become noticeably stronger.

We conclude by mentioning three caveats of this analysis. First, as noted above, KN models adopted here assume axial symmetry and a distribution over a 2π azimuthal angle for the dynamical ejecta. In reality, the dynamical ejecta are predicted to cover only $\sim$ half of the plane and thus $\sim$ half of the orientations in the equatorial plane are expected to be brighter than predicted here. Accounting for the predicted break of symmetry will therefore produce stronger constraints for equatorial viewing angles than those derived here. The second caveat follows from the fact that the composition of the post-merger ejecta in NSBH mergers is uncertain. This is due in large part to the very approximate treatment of neutrinos used in many simulations [50,51], but also to the fact that the post-merger ejecta may contain a number of independent components with different geometry, composition, and temperature [52–54], and the relative contribution of these various components is strongly affected by the unknown strength and large scale structure of the post-merger magnetic field [49]. Here we adopted a composition intermediate between lanthanide-poor and lanthanide-rich material but note that a different composition would lead to different constraints in the $M_{\rm ej,dyn} - M_{\rm ej,pm}$ parameter space. For instance, a lanthanide-poor composition for the post-merger ejecta is expected to lead to brighter KNe and thus to result in stronger constraints. Finally, a third caveat is that binaries leading to extremely massive ejecta are not rigorously excluded by our analysis. This is due to the fact that within the grid of models considered here, the more massive ejecta ($M_{\rm dyn} \gtrsim 0.07 M_\odot$ and $M_{\rm pm} \gtrsim 0.07 M_\odot$) lead to KN that evolve too slowly to pass the observational cuts that we impose on the time evolution of the magnitude of KN, and also because some extreme

low-mass systems may have $M_{\rm pm} \geq 0.1 M_\odot$, a region not covered by our grid of simulations. The small regions of parameter space untested by this study is shown in Extended Data Figure 9. We note that on this figure, the excluded region at high NS radii is due to the observational cuts; requiring observations to be sensitive to that region of parameter space may lead to many more false positives. The smaller region at low NS radii and low mass ratio is due to our $M_{\rm pm} < 0.1 M_\odot$ limit.

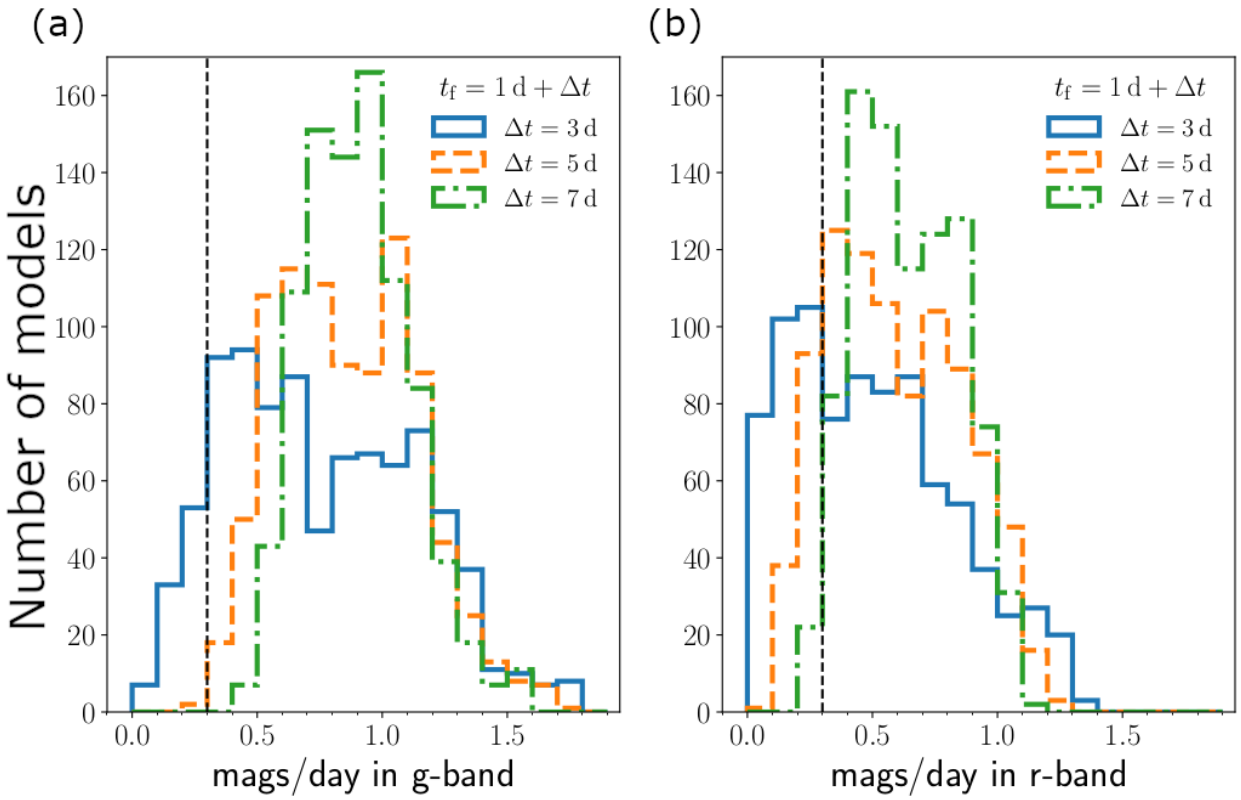

Supplementary Information Figure 2: **Plot of the decay rate (mag/day) in g-band (a) and r-band (b) for all the ejecta masses and viewing angles of the modeled grid.** Blue histograms are for time windows from 1 to 4 days after merger ($\Delta t = 3$ days), orange from 1 to 6 days ($\Delta t = 5$ days), green from 1 to 8 days ($\Delta t = 7$ days). In general, $96\,\%$ of models show faster decay than 0.3 mags/day (dashed vertical line) in g-band, while $82\,\%$ of models show faster decay than 0.3 mags/day in r-band. The more slowly fading models are the higher mass ones. Particularly, our threshold was chosen based on the 7 days baseline, as all the candidates meet that requirement.

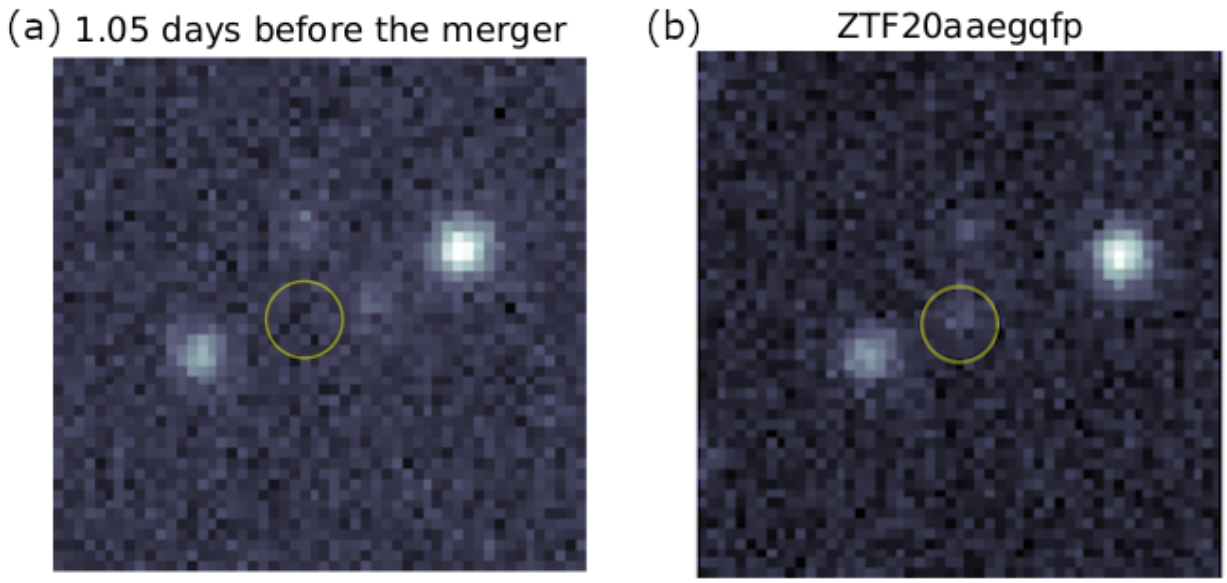

Supplementary Information Figure 3: **ZTF r-band cutouts of the slow moving asteroid ZTF20aaegqfp.** The yellow circles show the position of the ZTF candidate in both cutouts. Panel (a) shows a cutout of the region one day before the trigger. There, it is possible to see a source to the right of ZTF20aaegqfp position, marked with a yellow circle. This source was located at 7.3″ from our candidate. Panel (b) shows the discovery image of our candidate ZTF20aaegqfp, which is located within the circle. The cutouts are 0.7 sq. arcmin and north and east are up and to the left respectively.

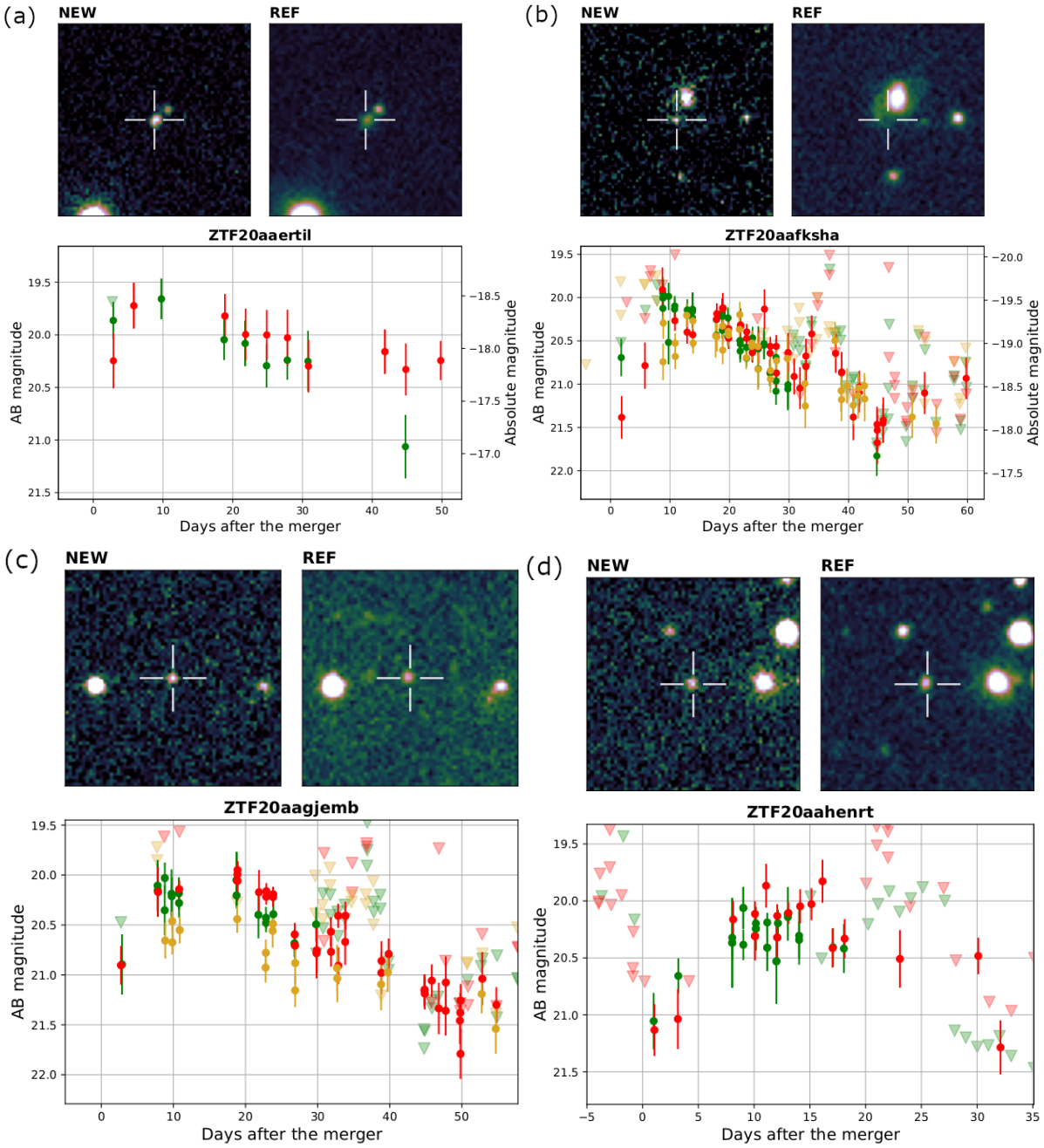

Supplementary Information Figure 4: **Lightcurves and r-band cutouts for a subset of the most well-sampled lightcurves for ZTF candidates that were ruled out photometrically.** Colors were used to represent the different bands: green, red and yellow for g-, r- and i- bands. The triangles in the lightcurve represent upper limits and filled circles are the detected magnitudes of the object. On each panel, the left cutout is the ZTF discovery image and the right one is the corresponding ZTF reference image. The transient is marked with a cross and the size of the cutouts is 0.7 sq. arcmin with north being up and east to the left. The candidates highlighted here are as follows: (a) ZTF20aaertil, (b) ZTF20aafksha, (c) ZTF20aagjemb, and (d) ZTF20aahenrt.

Supplementary Information Table 1: Follow-up table for all spectroscopically classified transients. Our spectra were obtained with GTC [27,28], ePESSTO [32], P60+SEDM, and P200+DBSP. The spectroscopic redshifts are listed as well. The objects with a star (*) were first reported to TNS by ALeRCE. Discovery magnitudes reported are extinction-corrected.

Name	RA	Dec	TNS	Discov. Mag.	Classification	Spec. facilities	Spec. Redshift
ZTF20aaertpj	14:27:52	33:34:10	AT2020pv*	$g = 19.88 \pm 0.16$	SN Ib	GTC	0.026
ZTF20aaervoa	15:02:38	16:28:22	AT2020pp*	$g = 20.63 \pm 0.30$	SN IIp	GTC	0.046
ZTF20aaervyn	15:01:27	20:37:24	AT2020pq*	$g = 20.62 \pm 0.26$	SN Ia	GTC	0.112
ZTF20aaerxsd	14:00:54	45:28:22	AT2020py	$g = 20.27 \pm 0.23$	SN Ia	GTC	0.055
ZTF20aaerqbx	15:49:26	40:49:55	AT2020ps*	$g = 19.46 \pm 0.15$	SN IIp	GTC	0.098
ZTF20aafanxk	05:35:36	11:46:15	AT2020adk	$r = 18.52 \pm 0.25$	SN Ia	P60+SEDM	0.133
ZTF20aafujqk	17:57:00	10:32:20	AT2020adg	$r = 18.17 \pm 0.10$	SN Ia	P60+SEDM	0.074
ZTF20aaevbzl	13:26:41	30:52:31	AT2020adf	$i = 19.31 \pm 0.24$	CV	P200+DBSP	0.0
ZTF20aafqpum	03:06:08	13:54:48	SN2020yo	$g = 19.76 \pm 0.20$	SN Ia 91-bg	ePESSTO	0.09

References

1. Bellm, E. C. *et al.* The zwicky transient facility: System overview, performance, and first results. *Pub. Astron. Soc. Pac.* **131**, 018002 (2018). URL https://doi.org/10.1088%2F1538-3873%2Faaecbe.

2. Masci, F. J. *et al.* The zwicky transient facility: Data processing, products, and archive. *Pub. Astron. Soc. Pac.* **131**, 018003 (2018).

3. Yao, Y. *et al.* ZTF early observations of type ia supernovae. i. properties of the 2018 sample. *Astrophys. J.* **886**, 152 (2019). URL http://dx.doi.org/10.3847/1538-4357/ab4cf5.

4. Almualla, M. *et al.* Dynamic scheduling: target of opportunity observations of gravitational wave events. *Mon. Not. R. Astron. Soc.* **495**, 4366–4371 (2020). URL https://doi.org/10.1093/mnras/staa1498. https://academic.oup.com/mnras/article-pdf/495/4/4366/33371783/staa1498.pdf.

5. Rana, J., Anand, S. & Bose, S. Optimal search strategy for finding transients in large-sky error regions under realistic constraints. *Astrophys. J.* **876**, 104 (2019). URL http://dx.doi.org/10.3847/1538-4357/ab165a.

Supplementary Information Table 2: Follow-up table of the candidates identified for S200105ae, reported in Ref. [25]. The ZTF objects with a star (*) in the TNS column were first reported to TNS by ALeRCE. The spectroscopic (s) or photometric (p) redshifts of the respective host galaxies are listed as well. As a reference, the all-sky averaged distance to the source is 283 ± 74 Mpc, corresponding to a redshift range z = 0.045–0.077. We use the same rejection criteria described in more detail in section 2 here, as follows: slow photometric evolution (slow), hostless, stellar, and slow moving asteroid (asteroid).

Name	RA	Dec	TNS	Discov. Mag.	Host/Redshift	rejection criteria
ZTF20aafduvt	03:36:29	−07:49:35	AT2020ado	g = 19.57 ± 0.29	0.25 ± 0.02 (p)	slow
ZTF20aaflndh	01:22:38	−06:49:34	AT2020xz	g = 19.11 ± 0.11	0.091 ± 0.023 (p)	slow
ZTF20aaexpwt	06:26:01	11:33:39	AT2020adi	r = 16.95 ± 0.17	-	slow
ZTF20aafukgx	18:23:21	17:49:32	AT2020adj	r = 18.40 ± 0.15	-	slow
ZTF20aagijez	15:04:13	27:29:04	AT2020adm	r = 19.67 ± 0.3	0.061 (s)	slow
ZTF20aagiiik	16:19:10	53:45:38	AT2020abl*	g = 19.76 ± 0.22	0.13 (s)	slow
ZTF20aafdxkf	03:42:07	−03:11:39	AT2020ads	r = 20.02 ± 0.25	-	slow
ZTF20aagiipi	15:33:25	42:02:37	AT2020adl	g = 20.10 ± 0.32	0.39 ± 0.02 (p)	slow
ZTF20aafsnux	14:36:01	55:11:49	AT2020dzu	g = 19.67 ± 0.22	-	slow
ZTF20aaertil	14:52:26	31:01:19	AT2020pu*	g = 19.86 ± 0.18	0.093 (s)	slow
ZTF20aafksha	13:43:54	38:25:14	AT2020adr	g = 20.06 ± 0.26	0.167 (s)	slow
ZTF20aagjemb	14:51:26	45:20:41	AT2020adh	r = 20.90 ± 0.02	0.21 ± 0.06 (p)	slow
ZTF20aafefxe	07:47:24	14:42:24	AT2020adt	g = 21.0 ± 0.18	0.09 ± 0.05 (p)	slow
ZTF20aafaoki	05:13:14	05:09:56	AT2020adq	r = 19.21 ± 0.28	-	slow
ZTF20aafexle	04:20:31	−09:30:28	AT2020adn	r = 19.67 ± 0.30	0.18 ± 0.02 (p)	stellar
ZTF20aaegqfp	07:49:02	12:29:26	AT2020dzt	r = 19.37 ± 0.27	-	asteroid

Supplementary Information Table 3: Follow-up table of the candidates identified for S200115j, reported in Ref. [29]. As a reference, the all-sky averaged distance to the source is 340 ± 79 Mpc, corresponding to a redshift range z = 0.056–0.089.

Name	RA	Dec	TNS	Discov. Mag.	Host/Redshift	rejection criteria
ZTF20aahenrt	09:32:53	72:23:06	AT2020axb	g = 20.55 ± 0.29	0.16 ± 0.04 (p)	slow
ZTF20aagjqxg	02:59:39	06:41:11	AT2020aeo	g = 20.65 ± 0.26	-	slow
ZTF20aahakkp	05:07:55	56:27:50	AT2020bbk	g = 15.67 ± 0.08	-	slow
ZTF20aafqulk	03:39:45	27:44:05	AT2020yp	g = 20.74 ± 0.21	-	stellar
ZTF20aafqvyc	03:47:58	38:26:32	AT2020yq	r = 20.39 ± 0.19	-	asteroid

6. Hook, I. *et al.* The gemini–north multi-object spectrograph: Performance in imaging, long-slit, and multi-object spectroscopic modes. *Pub. Astron. Soc. Pac.* **116**, 425–440 (2004).

7. Blagorodnova, N. *et al.* The SED Machine: A Robotic Spectrograph for Fast Transient Classification. *Pub. Astron. Soc. Pac.* **130**, 035003 (2018).

8. Wilson, J. C. *et al.* *A Wide-Field Infrared Camera for the Palomar 200-inch Telescope*, vol. 4841 of *Society of Photo-Optical Instrumentation Engineers Conference Series*, 451–458 (2003).

9. Coughlin, M. W. *et al.* The Kitt Peak Electron Multiplying CCD demonstrator. *Mon. Not. R. Astron. Soc.* **485**, 1412–1419 (2019). URL https://doi.org/10.1093/mnras/stz497. http://oup.prod.sis.lan/mnras/article-pdf/485/1/1412/27994954/stz497.pdf.

10. Bertin, E. & Arnouts, S. SExtractor: Software for source extraction. *Astron. Astrophys.* **117**, 393–404 (1996).

11. Chambers, K. C. *et al.* The Pan-STARRS1 Surveys. *arXiv e-prints* arXiv:1612.05560 (2016). 1612.05560.

12. Bertin, E. *Automatic Astrometric and Photometric Calibration with SCAMP*, vol. 351 of *Astron. Soc. Pac. Conf. Ser.*, 112–115 (2006).

13. Becker, A. Hotpants: High order transform of psf and template subtraction. *Astrophysics Source Code Library* (2015).

14. Alard, C. Image subtraction using a space-varying kernel. *Astron. Astrophys.* **144**, 363–370 (2000).

15. Steele, I. A. *et al.* The liverpool telescope: performance and first results **5489**, 679–692 (2004).

16. Fremling, C. *et al.* PTF12os and iPTF13bvn. Two stripped-envelope supernovae from low-mass progenitors in NGC 5806. *Astron. Astrophys.* **593**, A68 (2016).

17. De, K. *et al.* Palomar Gattini-IR: Survey Overview, Data Processing System, On-sky Performance and First Results. *Pub. Astron. Soc. Pac.* **132**, 025001 (2020).

18. Bertin, E. *et al.* The TERAPIX Pipeline. In Bohlender, D. A., Durand, D. & Handley, T. H. (eds.) *Astronomical Data Analysis Software and Systems XI*, vol. 281 of *Astronom. Soc. Pac. Conf. Ser.*, 228 (2002).

19. Skrutskie, M. F. *et al.* The Two Micron All Sky Survey (2MASS). *Astrophys. J.* **131**, 1163–1183 (2006).

20. Schlafly, E. F. & Finkbeiner, D. P. Measuring reddening with sloan digital sky survey stellar spectra and recalibrating sfd. *Astrophys. J.* **737**, 103 (2011).

21. Rigault, M. *et al.* Fully automated integral field spectrograph pipeline for the sedmachine: pysedm. *Astron. Astrophys.* **627**, A115 (2019). URL http://dx.doi.org/10.1051/0004-6361/201935344.

22. Blondin, S. & Tonry, J. L. Determining the type, redshift, and age of a supernova spectrum. *Astrophys. J.* **666**, 1024–1047 (2007). URL http://dx.doi.org/10.1086/520494.

23. Bellm, E. C. & Sesar, B. pyraf-dbsp: Reduction pipeline for the Palomar Double Beam Spectrograph (2016). 1602.002.

24. Stein, R. *et al.* LIGO/Virgo S200105ae: Candidates from the Zwicky Transient Facility. *GRB Coordinates Network* **26673**, 1 (2020).

25. Ahumada, T. *et al.* LIGO/Virgo S200105ae: More candidates from the Zwicky Transient Facility. *GRB Coordinates Network* **26810**, 1 (2020).

26. Dey, A. *et al.* Overview of the desi legacy imaging surveys. *Astron. J.* **157**, 168 (2019). URL http://dx.doi.org/10.3847/1538-3881/ab089d.

27. Castro-Tirado, A. J. *et al.* LIGO/Virgo S200105ae: AT2020pq, AT2020ps and AT2020pv 10.4m GTC spectroscopy. *GRB Coordinates Network* **26703** (2020).

28. Valeev, A. F. *et al.* LIGO/Virgo S200105ae: AT2020pp and AT2020py 10.4m GTC spectroscopy. *GRB Coordinates Network* **26702** (2020).

29. Anand, S. *et al.* LIGO/Virgo S200115j: Candidates from the Zwicky Transient Facility. *GRB Coordinates Network* **26767**, 1 (2020).

30. Evans, P. A. *et al.* LIGO/Virgo S200115j: Swift-XRT sources. *GRB Coordinates Network* **26798**, 1 (2020).

31. Andreoni, I., Kasliwal, M. M., Cenko, S. B. & Yao, Y. LIGO/Virgo S200115j: Zwicky Transient Facility search for optical counterparts to Swift X-ray sources. *GRB Coordinates Network* **26863**, 1 (2020).

32. Schulze, S., Irani, I., Zimmerman, E., Bruch, R. & Yaron, O. ePESSTO+ Transient Classification Report for 2020-01-16. *Transient Name Server Classification Report* **2020-160**, 1 (2020).

33. Green, R. M. *Spherical Astronomy* (1985).

34. Jedicke, R., Bolin, B., Granvik, M. & Beshore, E. A fast method for quantifying observational selection effects in asteroid surveys. Icarus **266**, 173–188 (2016).

35. De, K., Hankins, M. & Kasliwal, M. M. LIGO/Virgo S200115j: NIR upper limits for ZTF20aafqvyc/AT2020yq from the Palomar 200-inch telescope. *GRB Coordinates Network* **26814**, 1 (2020).

36. Ahumada, T., Coughlin, M. & Anand, S. LIGO/Virgo S200115j: LCO upper limits for ZTF20aafqvyc/AT2020yq from the McDonald Observatory 1-m telescope. *GRB Coordinates Network* **26817**, 1 (2020).

37. Mazaeva, E., Pozanenko, A., Belkin, S., Klunko, E. & Volnova, A. LIGO/Virgo S200115j: Mondy upper limits for ZTF20aafqvyc/AT2020yq. *GRB Coordinates Network* **26819**, 1 (2020).

38. Ahumada, T. & Singer, L. LIGO/Virgo S200115j: GMOS-N upper limits for ZTF20aafqvyc/AT2020yq from the Gemini Observatory. *GRB Coordinates Network* **26822**, 1 (2020).

39. Coughlin, M. W. *et al.* Constraints on the neutron star equation of state from AT2017gfo using radiative transfer simulations. *Mon. Not. R. Astron. Soc.* **480**, 3871–3878 (2018). URL `http://dx.doi.org/10.1093/mnras/sty2174./oup/backfile/content_public/journal/mnras/480/3/10.1093_mnras_sty2174/1/sty2174.pdf`.

40. Coughlin, M. W., Dietrich, T., Margalit, B. & Metzger, B. D. Multimessenger Bayesian parameter inference of a binary neutron star merger. *Mon. Not. R. Astron. Soc.: Letters* **489**, L91–L96 (2019). URL https://doi.org/10.1093/mnrasl/slz133. http://oup.prod.sis.lan/mnrasl/article-pdf/489/1/L91/30032497/slz133.pdf.

41. Coughlin, M. W. *et al.* Implications of the search for optical counterparts during the first six months of the Advanced LIGO's and Advanced Virgo's third observing run: possible limits on the ejecta mass and binary properties. *Mon. Not. R. Astron. Soc.* **492**, 863–876 (2019). URL https://doi.org/10.1093/mnras/stz3457. https://academic.oup.com/mnras/article-pdf/492/1/863/31760484/stz3457.pdf.

42. Andreoni, I. *et al.* GROWTH on S190814bv: Deep Synoptic Limits on the Optical/Near-infrared Counterpart to a Neutron StarBlack Hole Merger. *Astrophys. J.* **890**, 131 (2020).

43. Dietrich, T. *et al.* New constraints on the supranuclear equation of state and the hubble constant from nuclear physics – multi-messenger astronomy (2020). 2002.11355.

44. Coughlin, M. W. *et al.* Implications of the search for optical counterparts during the second part of the advanced ligo's and advanced virgo's third observing run: lessons learned for future follow-up observations (2020). 2006.14756.

45. Foucart, F., Hinderer, T. & Nissanke, S. Remnant baryon mass in neutron star-black hole mergers: Predictions for binary neutron star mimickers and rapidly spinning black holes. *Phys. Rev.* **D98**, 081501 (2018).

46. Krüger, C. J. & Foucart, F. Estimates for disk and ejecta masses produced in compact binary mergers. *Physical Review D* **101**, 103002 (2020). URL http://dx.doi.org/10.1103/PhysRevD.101.103002.

47. Foucart, F. Black-hole-neutron-star mergers: Disk mass predictions. *Phys. Rev. D* **86**, 124007 (2012).

48. Kawaguchi, K., Kyutoku, K., Shibata, M. & Tanaka, M. Models of Kilonova/macronova Emission From Black Hole–neutron Star Mergers. *Astrophys. J.* **825**, 52 (2016).

49. Christie, I. M. *et al.* The Role of Magnetic Field Geometry in the Evolution of Neutron Star Merger Accretion Discs. *Mon. Not. R. Astron. Soc.* **490**, 4811–4825 (2019).

50. Wanajo, S. *et al.* Production of all the r-process nuclides in the dynamical ejecta of neutron star mergers. *Astrophys. J. Lett.* **789**, L39 (2014). URL http://stacks.iop.org/2041-8205/789/i=2/a=L39.

51. Foucart, F. *et al.* Evaluating radiation transport errors in merger simulations using a Monte Carlo algorithm. *Phys. Rev.* **D98**, 063007 (2018).

52. Kiuchi, K. *et al.* High resolution magnetohydrodynamic simulation of black hole-neutron star merger: Mass ejection and short gamma ray bursts. *Phys. Rev. D* **92**, 064034 (2015). URL https://link.aps.org/doi/10.1103/PhysRevD.92.064034.

53. Siegel, D. M. & Metzger, B. D. Three-dimensional general-relativistic magnetohydrodynamic simulations of remnant accretion disks from neutron star mergers: Outflows and r-process nucleosynthesis. *Phys. Rev. Lett.* **119**, 231102 (2017). URL http://dx.doi.org/10.1103/PhysRevLett.119.231102.

54. Fernández, R., Tchekhovskoy, A., Quataert, E., Foucart, F. & Kasen, D. Long-term GRMHD simulations of neutron star merger accretion discs: implications for electromagnetic counterparts. *Mon. Not. R. Astron. Soc.* **482**, 3373–3393 (2019).